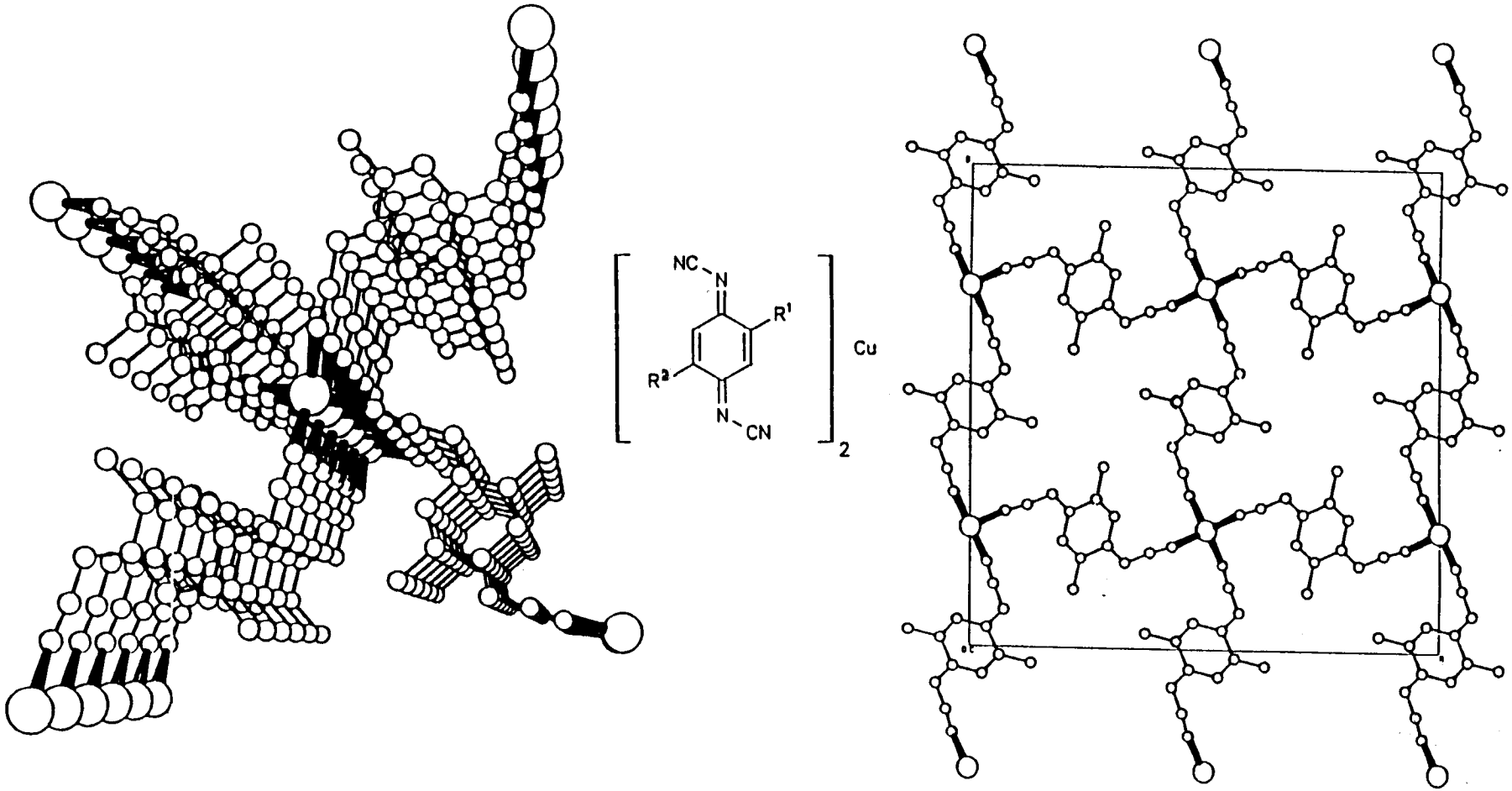

Fig. 1. Crystal lattice of $[R^1,R^3\text{-DCNQI}]_2Cu$.

View along one chain of copper ions with four stacks of ligands (c-axis).

Copper ions connected by bridges of ligands (a,b-plane).

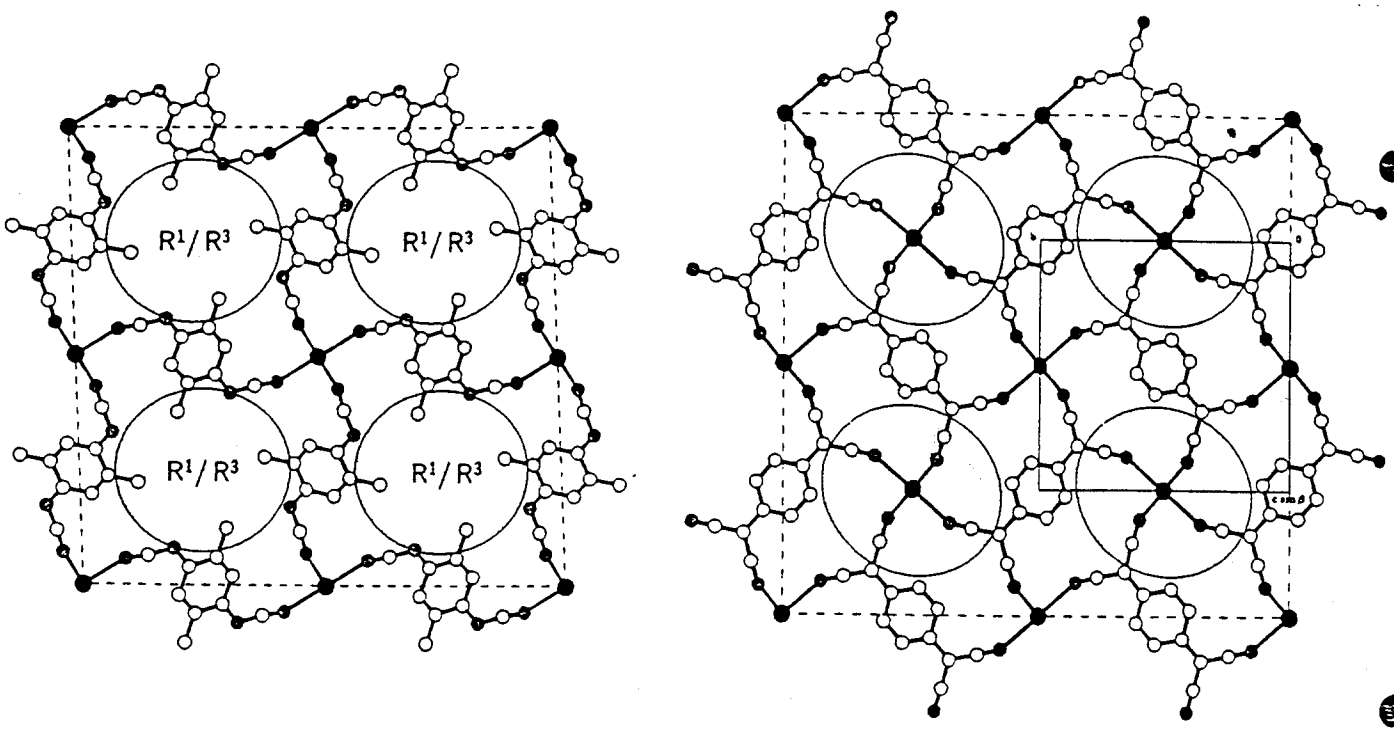

Fig. 2. Comparison of the crystal packing in $[R^1,R^3\text{-DCNQI}]_2Na$[9] (left) and TCNQ• Na[10] (right).

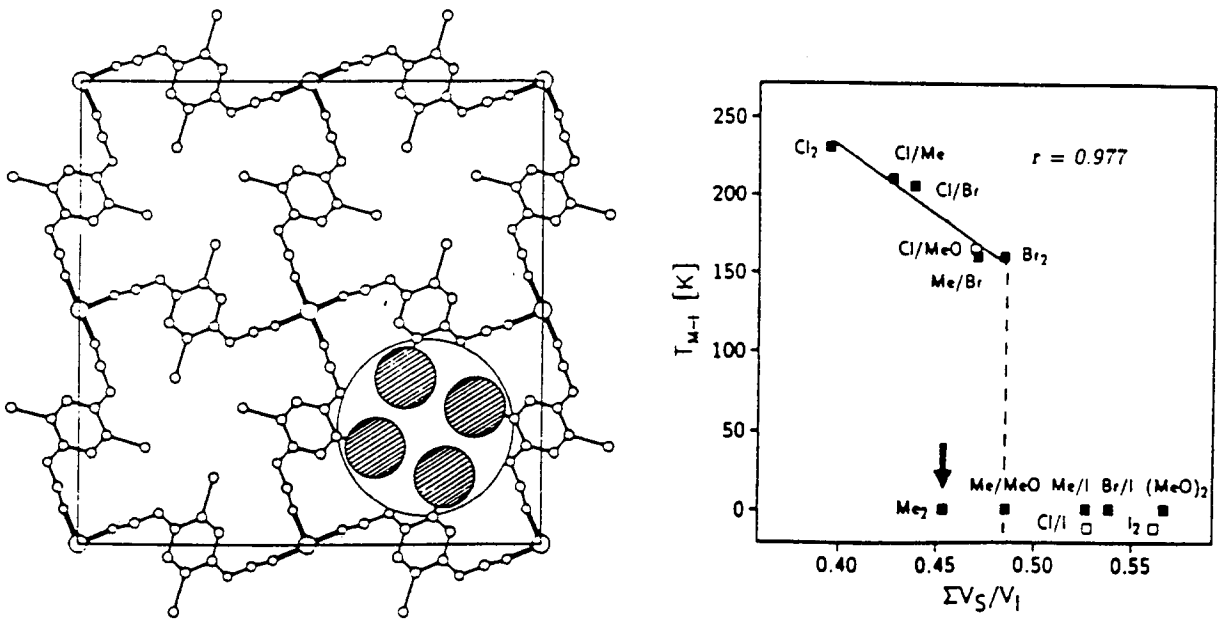

Fig. 5. Dependence of the phase transition temperature $T_{M\rightarrow I}$ of $[R^1,R^3\text{-DCNQI}]_2Cu$ on the volume of the substituents R^1 and R^3.

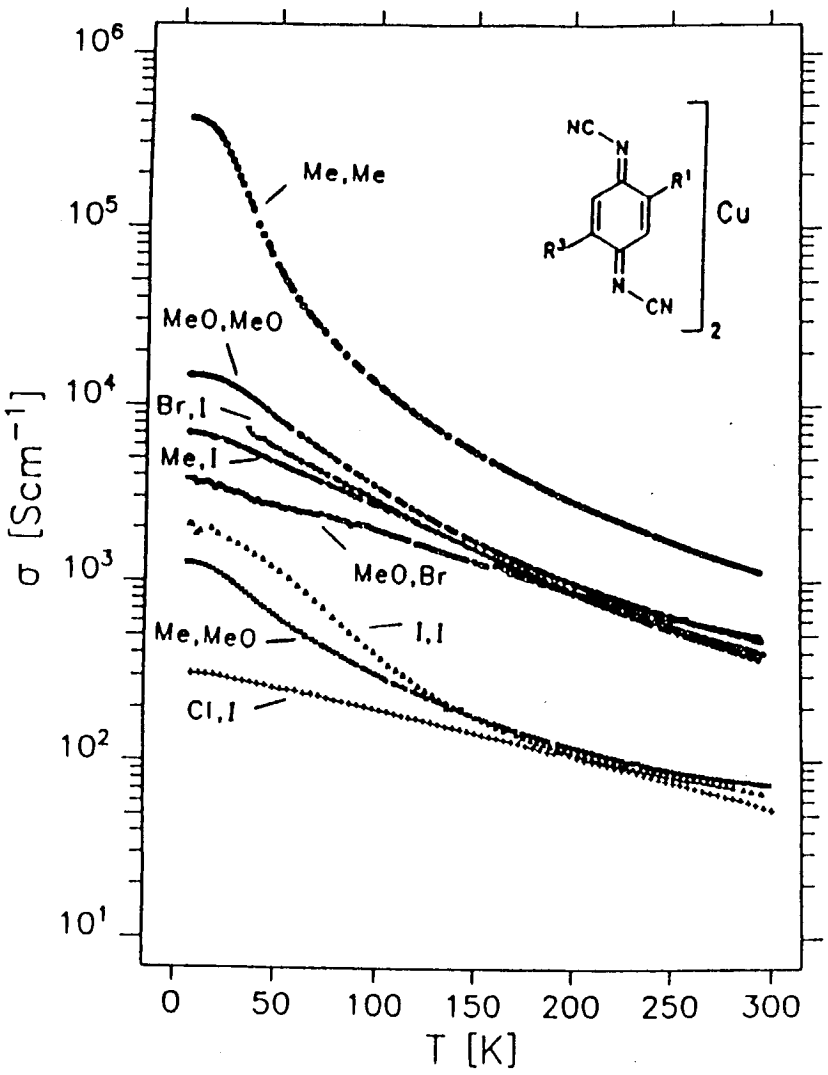

Fig. 3. Temperature dependence of conductivity of DCNQI copper salts without phase transitions.

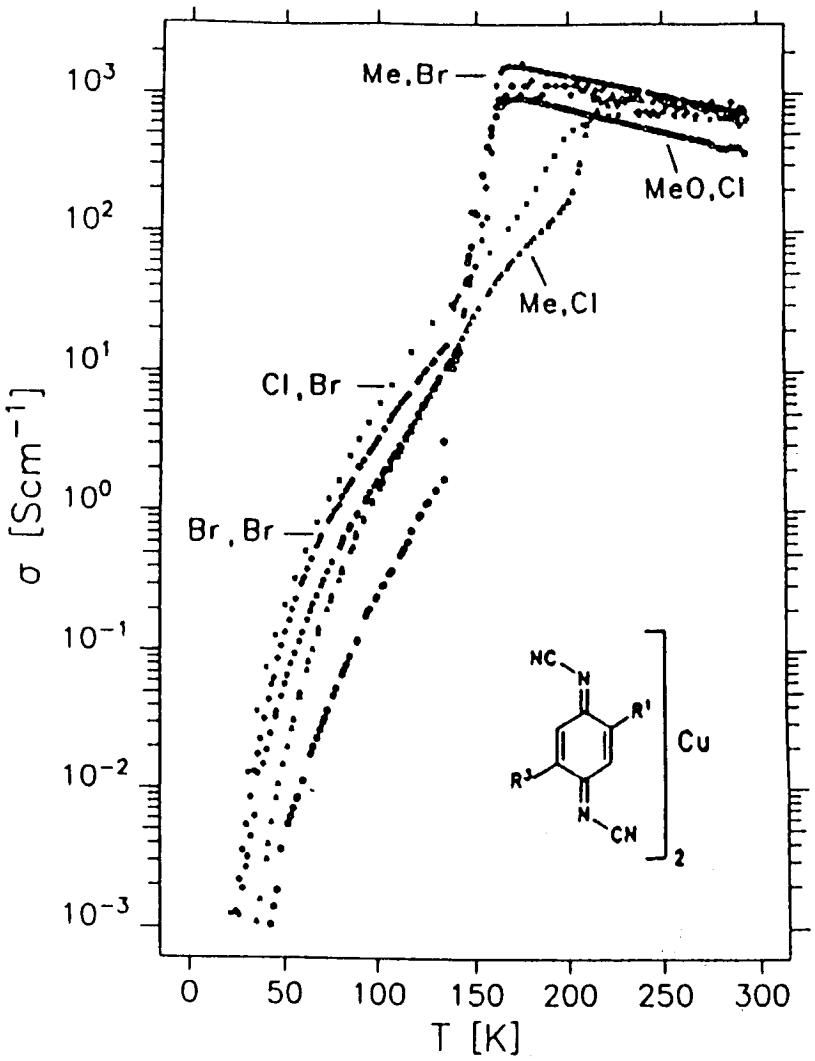

Fig. 4. Temperature dependence of conductivity of DCNQI copper salts with phase transitions.

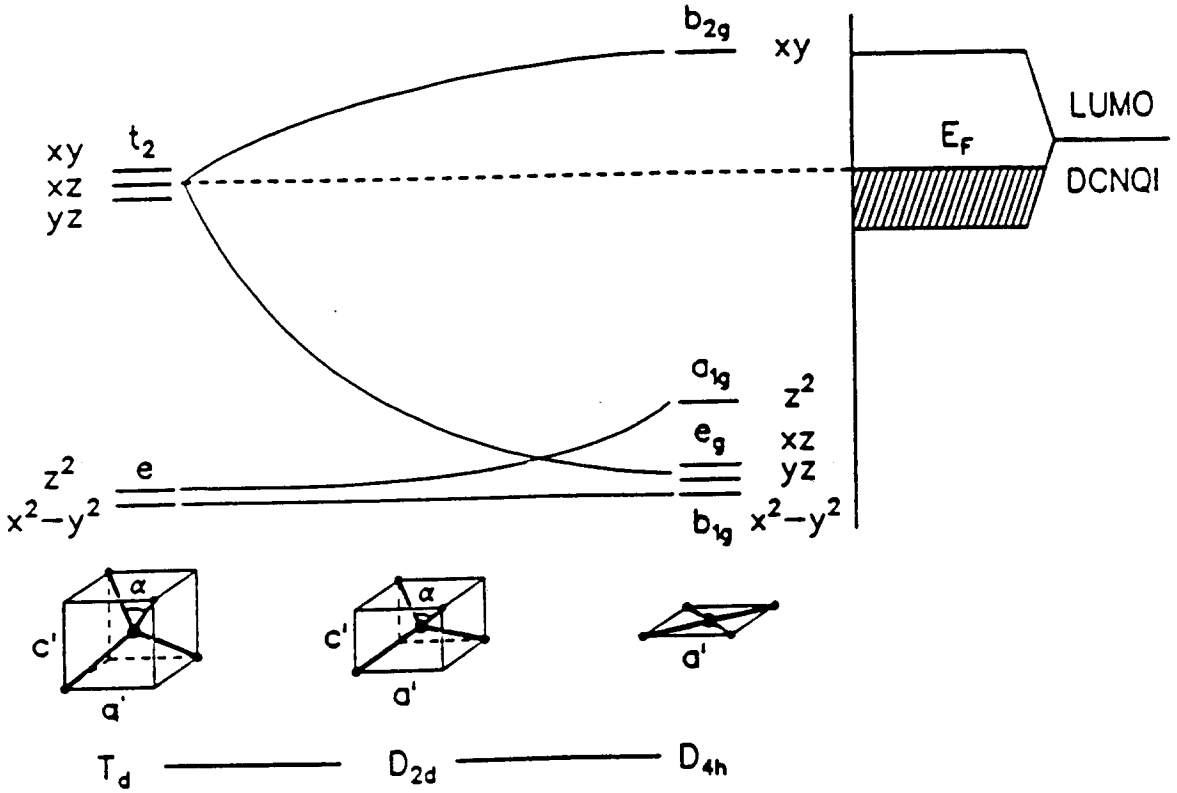

Fig. 6. Schematic presentation of the orbital energies of copper, dependent on the geometry in connection with the Fermi energy of the DCNQI band.

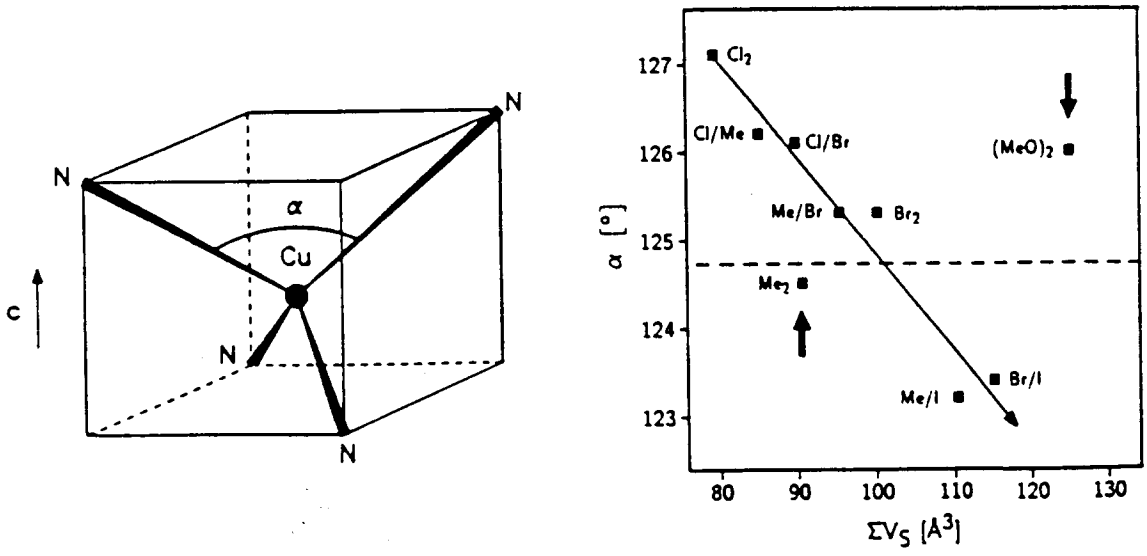

Fig. 7. Correlation of coordination angles α with substituent volumes of R^1 and R^3 in $[R^1,R^3\text{-DCNQI}]_2Cu$.

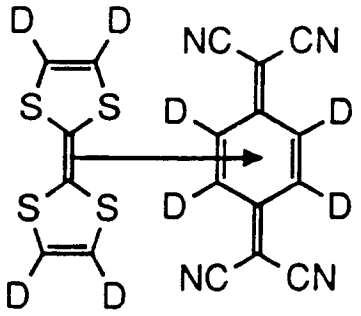

ΔT_p = +0.75 K
J.R. Cooper et al.
1978

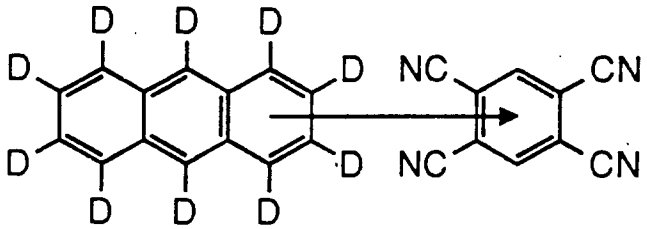

ΔT_p = -15 K
D.F. Williams et al.
1980

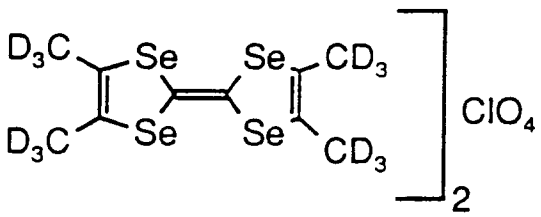

ΔT_c = -0.09 K
F. Wudl et al.
1984

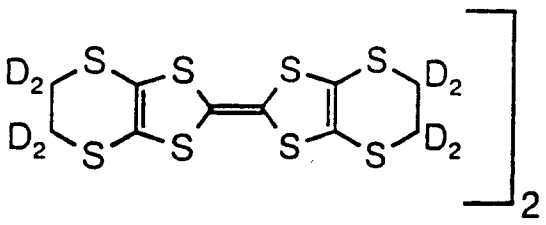

I_3

ΔT_c = +0.28 K
D. Schweitzer et al.
1986

$XCu(NCN)_2$

ΔT_c ~ +1.2 K
G. Saito et al.
1993

Fig. 8. Deuterium effects on phase transition (T_p) and superconduction (T_c) of various CT-complexes and radical cation salts compared to their undeuterated counterparts.

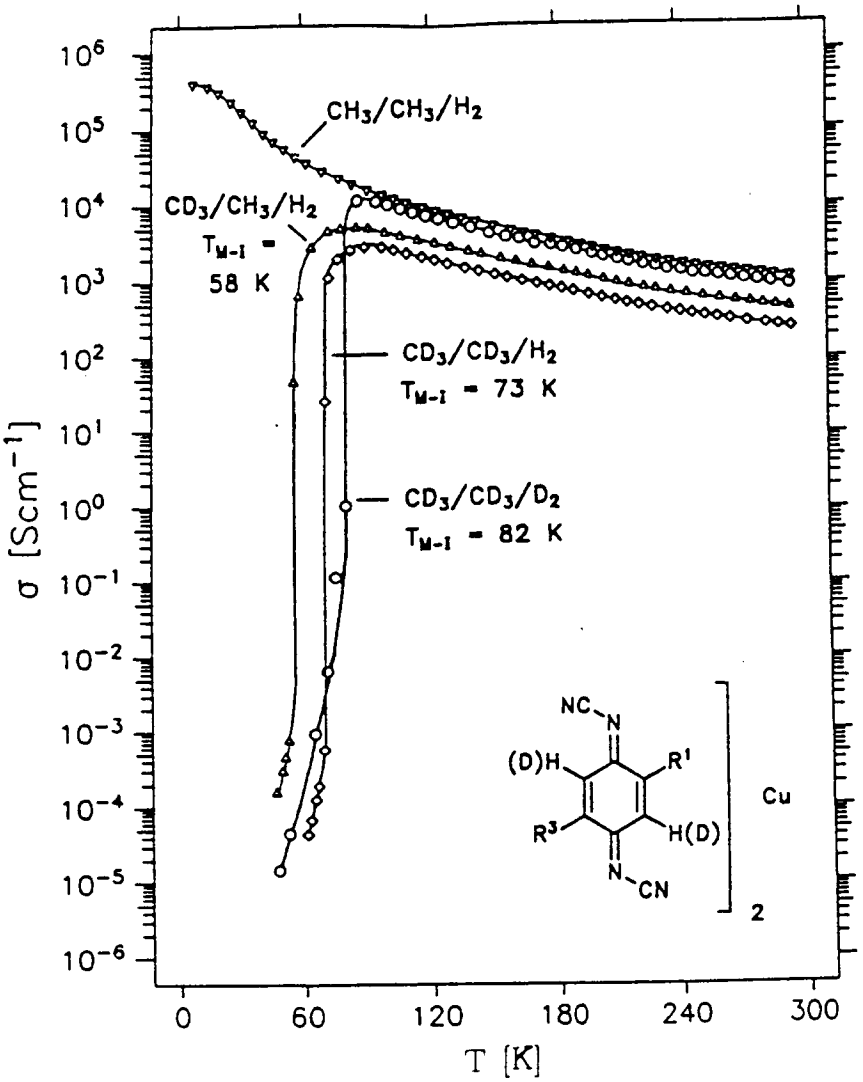

Fig. 9. Effect of H/D-exchange on the temperature dependend conductivities of [2,5-Me_2DCNQI]$_2$Cu (**1a - 1d**).

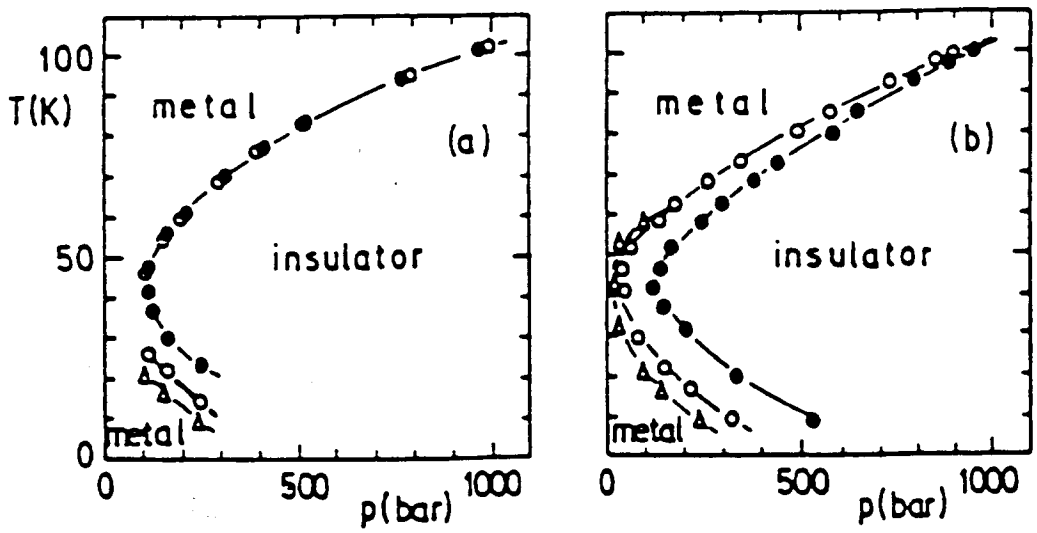

Fig. 10. Pressure induced phase transitions of [2,5-Me_2DCNQI]$_2$Cu on cooling. The low pressure phase diagram of (DM-DCNQI)$_2$Cu (a) p fixed, T variable. Open and full circles: cooling and warming, respectively: open triangles: the first cooling only. (b) T fixed, p variable. Open and full circles: decreasing and increasing pressure, respectively; open triangles: the first pressure decrease[20].

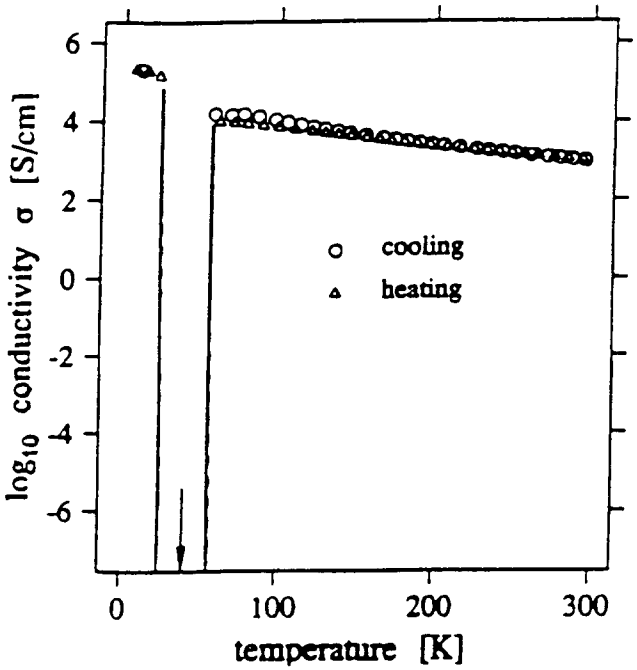

Fig. 11. Temperature dependent conductivity of $[2,5\text{-}Me_2DCNQI]_2Cu$ D_6/H_8 alloy 30:70

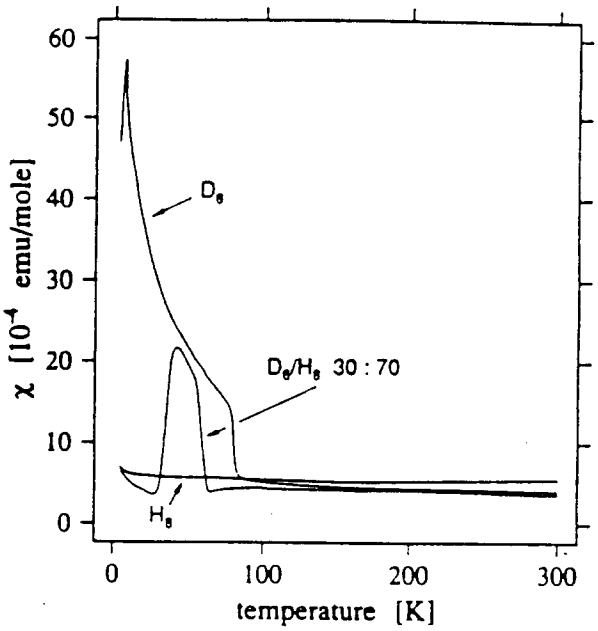

Fig. 12. Temperature dependent susceptibilities of $[2,5\text{-}Me_2DCNQI]_2Cu$ H_8 (**1a**), D_6 (**1c**) and D_6/H_8 alloy 30:70

	X = H	X = D
$d_{\pi\text{-}\pi}$	- 2.12%	- 2.68%
c-axis	- 2.29%	- 2.53%
a,b-axis	+ 0.22%	+ 0.34%
V	- 1.86%	- 1.88%
α_{Co}N-Cu-N	+ 1.5°	+ 3.5°
	metal	semicond.

phase trans.

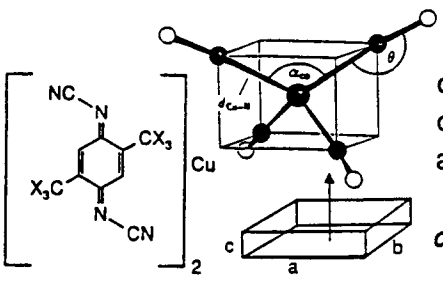

	X = H → X = D	
$d_{\pi\text{-}\pi}$	- 0.15%	
c-axis	- 0.17%	
a,b-axis	+ 0.06%	
V	- 0.05%	
α_{Co}N-Cu-N	124.8°	124.8°

Fig. 13. Differences of critical crystal data at ambient temperature between **1a** (X=H) and **1c** (X=D)

Fig. 14. Differences of critical crystal data between room temperature and 20 K

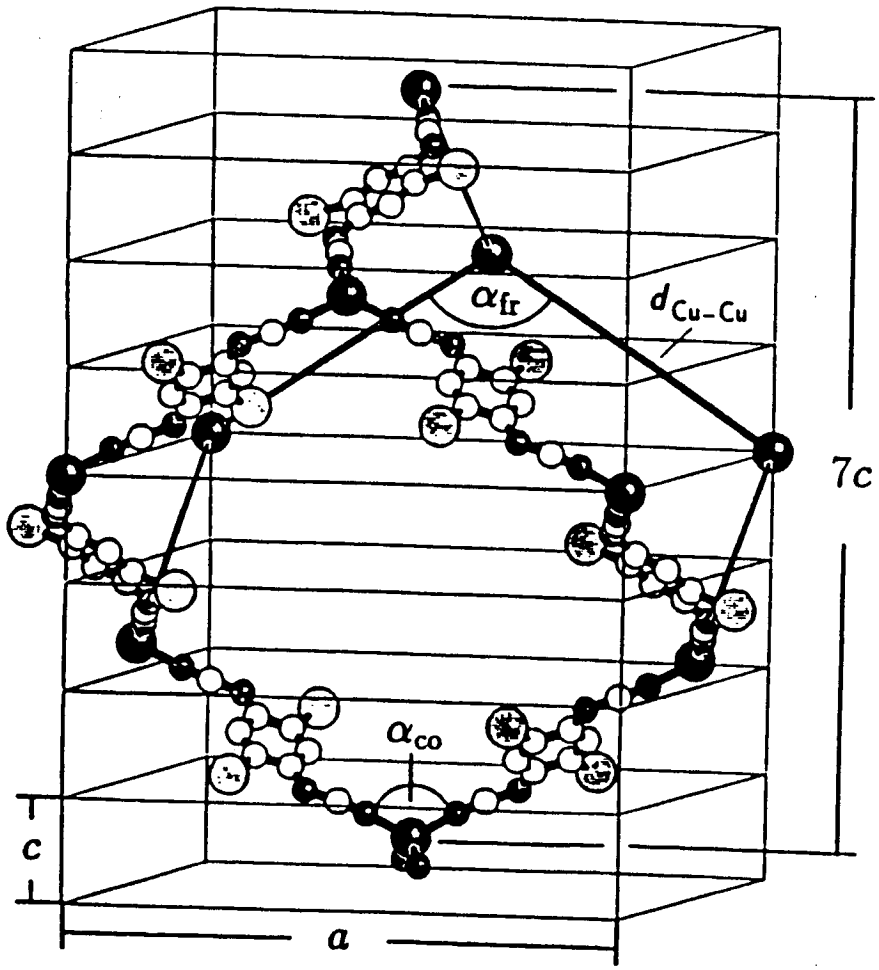

Fig. 15. A superadamantane unit in the crystal lattice of $[2,5\text{-}Me_2DCNQI]_2Cu$. The distance 7c encloses two Cu ions of the same column

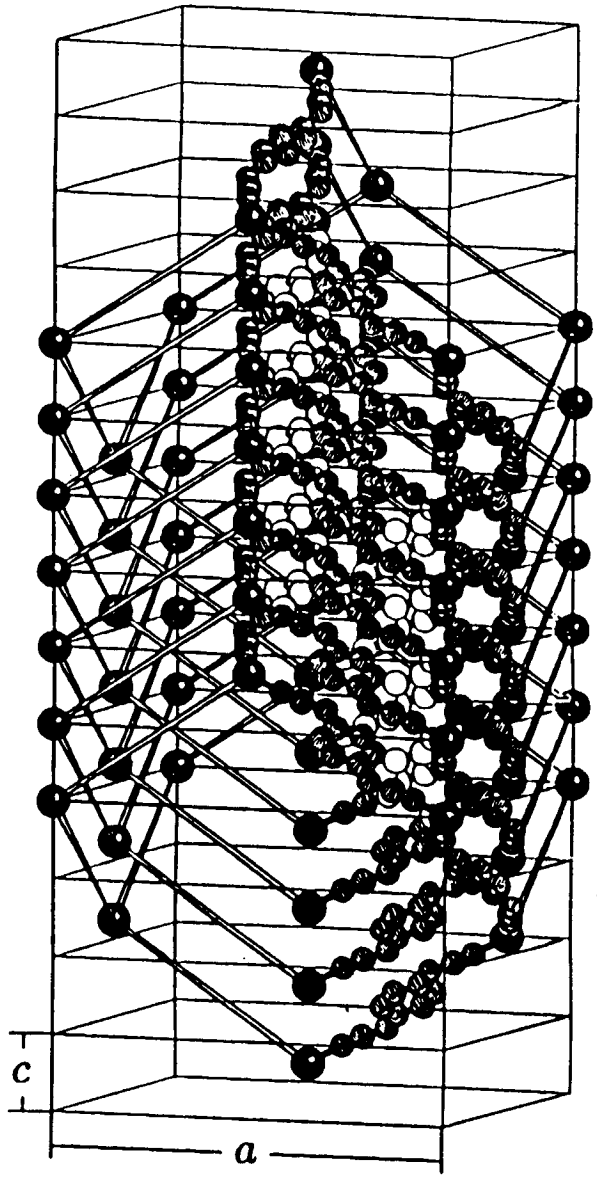

Fig. 16. Seven intercalating superadamantane units in the crystal lattice of $[2,5\text{-}Me_2DCNQI]_2Cu$

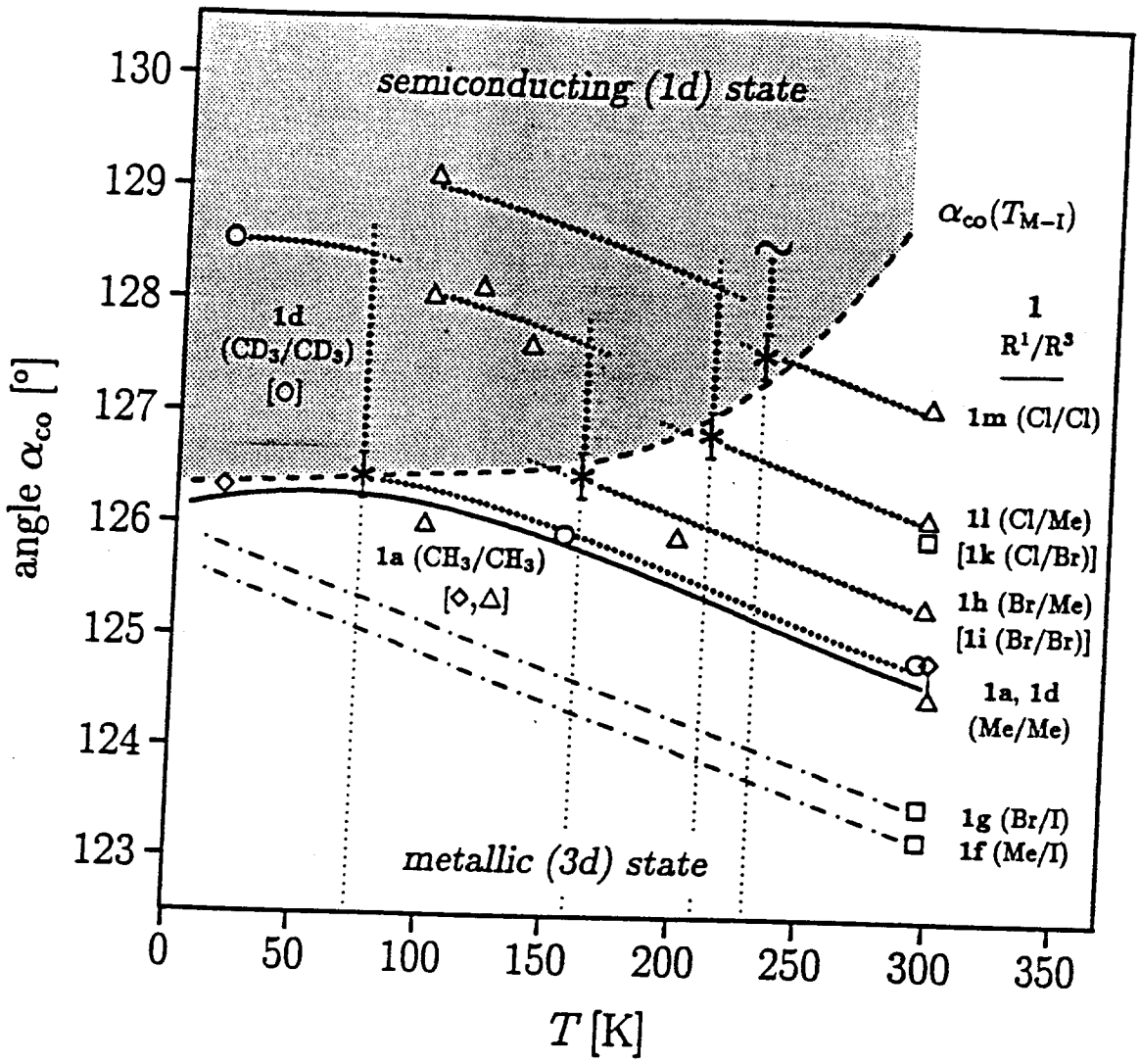

Fig. 17. Correlation of the temperature dependent threshold coordination angle α_{co} with the substituent pattern in $[R^1,R^3\text{-DCNQI}]_2Cu$.